Growth and Reactivity of Titanium Oxide Ultrathin Films on Ni(110)

ARTICLE *in* THE JOURNAL OF PHYSICAL CHEMISTRY C · MAY 2007

Impact Factor: 4.77 · DOI: 10.1021/jp067802m

Growth and Reactivity of Titanium Oxide Ultrathin Films on Ni(110)

Anthoula Chrysa Papageorgiou,[†] Gregory Cabailh,[†] Qiao Chen,[†] Andrea Resta,[‡] Edvin Lundgren,[‡] Jesper N. Andersen,[‡] and Geoff Thornton*,[†]

London Centre for Nanotechnology and Chemistry Department, University College London, 17-19 Gordon Street, London WC1H 0AH, UK, and Department of Synchrotron Radiation Research, Institute of Physics, Lund University, Box 118, S-221 00 Lund, Sweden

Received: November 23, 2006; In Final Form: March 19, 2007

Soft X-ray photoelectron spectroscopy (SXPS) and X-ray absorption near-edge structure (XANES) have been combined with low-energy electron diffraction (LEED) to examine the growth of titanium dioxide thin films on Ni(110). Depending on the initial titanium coverage, the formation of two different films is observed, a quasi-hexagonal phase and a film with rutile (110) rods. Spectroscopy (SXPS and XANES) results indicate that all films consist of fully oxidized titanium. Furthermore, the reactivity of the higher coverage phase, consisting partly of rutile TiO_2(110), was investigated after exposure to molecular water at 190 K. The formation of molecular water and hydroxyls was observed for low-pressure exposure (less than 10^{-7} mbar). High-pressure exposure (on the order of 10^{-6} mbar) resulted in hydroxylation of the thin film, which was found to be reversible upon annealing.

1. Introduction

Thin oxide films have been the subject of numerous studies in the past few decades.[1] In particular, intense efforts have been made to elucidate, on the atomic scale, the interface between metals and oxides. This interest is fueled by the quest to find nanostructures which can be exploited in electronic devices, by the importance of thin oxide films as corrosion inhibitors,[2] and by the use of thin oxide films as models for the catalyst supports.[3−5] Moreover, thin oxide films can act as mimics of the native surfaces, with the advantage that the metallic substrate provides the necessary conductivity required for some characterization techniques. For most systems, attention has focused on the characterization of the coverage/oxidation surface phase diagram, with more recent studies probing their reactivity.[6]

Titanium dioxide, and in particular its most stable surface, the rutile (110) plane (Figure 1c), is considered the "prototypical" oxide[7] and has been extensively investigated in surface science. Our work was inspired by an early study of the growth of titania on $Ni_{94}Ti_6$(110) alloy, which demonstrated, by X-ray photoelectron diffraction (XPD) measurements, the presence of rutile TiO_2(110).[2] Previous work confirms that similar thin titanium oxide films can be formed without using NiTi alloys by instead depositing Ti onto pure Ni(110) surfaces.[8−10] To our knowledge, bulk-like rutile TiO_2 films have not been reported to grow in the ultrathin limit on any other metallic substrate. In the present study, we employed synchrotron radiation soft X-ray photoelectron spectroscopy (SXPS) and X-ray absorption near-edge structure (XANES) combined with low-energy electron diffraction (LEED) to characterize the growth of ultrathin films of TiO_x.

In addition to the structural characterization, we have investigated the reactivity of the rutile thin film using H_2O as a probe and compared this behavior with that of the (110) surface of a rutile TiO_2 single crystal. For ideal rutile TiO_2-(110), theoretical calculations have predicted that dissociation

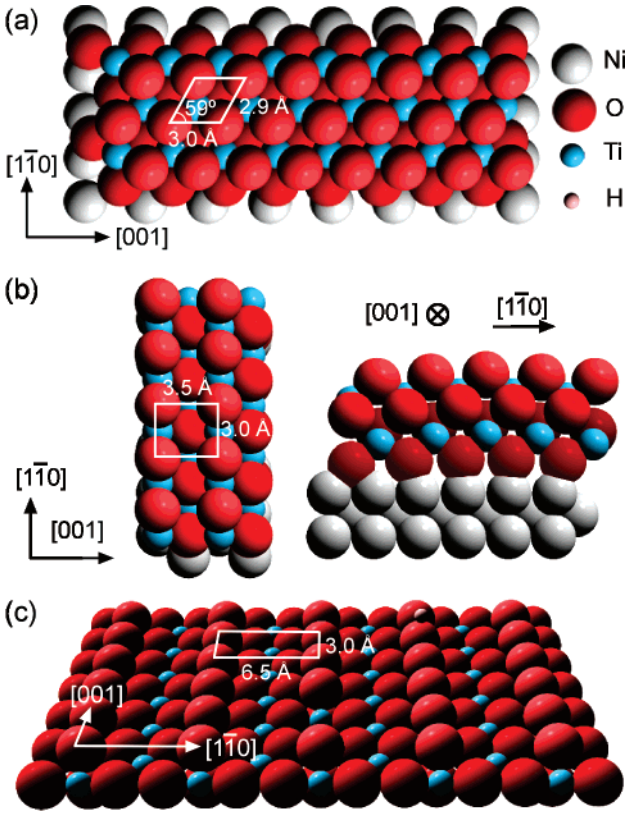

Figure 1. Models of the surfaces. (a) Model of the TiO_2 quasi-hexagonal phase grown on Ni(110), as proposed by Atrei et al.[2] The unit cell is indicated. The axes display the orientation of the substrate. (b) Top and side view of a proposed model for the wetting layer phase grown on Ni(110). The unit cell is indicated. The axes display the orientation of the substrate. (c) A model of the rutile TiO_2(110) surface, as typically prepared in UHV, containing an OH group and an oxygen vacancy. The unit cell and the high symmetry axes are displayed.

* To whom correspondence should be addressed. Tel.: +44 20 7679 7979. Fax: +44 20 7679 0595. E-mail: g.thornton@ucl.ac.uk.
[†] University College London.
[‡] Lund University.

10.1021/jp067802m CCC: $37.00
Published on Web 05/10/2007

of H_2O is thermodynamically favorable, but there is an energy barrier associated with the mobility of H_2O on the surface.[11]

The interaction of water with an oxide depends critically upon the partial pressure of water during exposure. Several ultrahigh vacuum (UHV) experiments on TiO_2(110) suggest that H_2O adsorbs molecularly in the absence of oxygen vacancies.[12−14] These vacancies do dissociate H_2O at room temperature to typically give ∼10% ML (1 monolayer is equivalent to the number of surface unit cells) of OH.[12,15] In contrast to the UHV regime, at pressures $>10^{-6}$ mbar, the selvedge of TiO_2(110) is known to hydroxylate.[16,17]

2. Experimental Section

The measurements reported here employed beamline I311 at MAX-lab II.[18] The synchrotron radiation light was incident at 45°, with the electric vector lying in the [1$\bar{1}$0] azimuth of the Ni(110) substrate. Photoelectrons were collected at normal emission using a hemispherical SCIENTA-SES200 electron energy analyzer. The end station was operated at a base pressure of $<10^{-10}$ mbar and was equipped with a LEED system, a homemade electron beam Ti doser, and standard facilities for crystal preparation and molecule dosing.

The Ni(110) surface was prepared by cycles of argon sputtering and annealing to 1070 K until a sharp (1 × 1) LEED pattern was obtained and no contamination was detected by SXPS. All LEED patterns were recorded at room temperature. Ultrathin films of TiO_x were grown in situ as follows. Ti was deposited on the substrate held at room temperature in vacuum, subsequently oxidized in a flow of 1×10^{-7} mbar of O_2, and annealed at 800 K. Water was double distilled and purified by freeze−pump−thaw cycles. The water was dosed at a sample temperature of 190 K using two different pressure regimes, 10^{-8} and 10^{-6} mbar.

The XANES spectra presented in this article were obtained by measuring the partial electron yield as a function of photon energy scanned through the Ti $L_{2,3}$-edge. All XANES experiments were performed at room temperature. The kinetic energy range was calibrated by referring to the positions of the first- and second-order excitations of the Ni 3p core levels.

Regarding the SXPS spectra, the binding energy scale was calibrated with respect to the Fermi energy of the nickel crystal since the films were thin enough to allow the detection of nickel in the valence band spectra. The Ni 2p, O 1s, and Ti 2p core levels were excited with photon energies of 1000, 650, and 680 eV, respectively. SXPS spectra were recorded at room temperature unless otherwise stated. The raw core level spectra were fitted using a sum of Voigt-type functions. The width of the Lorentzian or Doniach−Šunjić (used where appropriate[19]) contribution to the peaks was kept constant. The width of the Gaussian contribution was allowed to vary, accounting for temperature effects. A Shirley-plus-polynomial fit was used to model the background,[20] using a least-squares method to optimize the fits.

The possibility of photon beam modification of adsorbed H_2O has recently been studied by Weissenrieder et al. for Ru{0001}[21] using beamline I311 at MAX-lab II. This is the same beamline as employed in the present work. They report a photon current of $(5-10) \times 10^{10}$ ph•s^{-1} into the area of the focused photon beam, 0.3×1.0 mm^2. This is smaller by a factor of 3.3 than the flux reported in earlier work on H_2O on TiO_2(110),[14] where no photon-induced dissociation was observed after exposure to the photon beam for about an hour. On this basis, we can assume that there is no beam-induced dissociation in the present experiments.

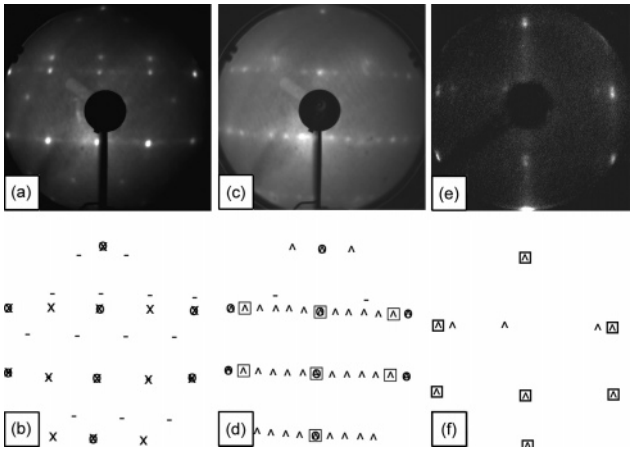

Figure 2. (a) LEED pattern (128 eV) of the quasi-hexagonal phase (subMLE Ti annealed to 800 K for 30 min in 10^{-7} mbar of O_2) compared with (b) a schematic representation of the diffraction pattern. (c) LEED pattern of the rutile TiO_2(110) overlayer (5 MLE of Ti oxidized for 1 min in 10^{-7} mbar of O_2 and annealed to 800 K) recorded on the beamline end station (123 eV) with (d) the corresponding schematic representation of the diffraction pattern. (e) LEED pattern of the rutile TiO_2(110) overlayer (2.5 MLE of Ti annealed to 800 K for 30 min in 10^{-7} mbar of O_2) obtained on LT-STM (58 eV) with (f) the corresponding schematic representation of the diffraction pattern. Circles mark the periodicity of Ni(110), crosses mark a (2 × 1) periodicity of the Ni substrate, "−" marks the quasi-hexagonal structure, squares indicate the periodicity of the wetting layer, and "∧" spots show its multiple diffraction spots and/or a coincidence cell between the wetting layer and the substrate. The TiO_2(110) contribution is evident along its [001] azimuth, along which it coincides with the wetting layer. No spots are observed in the TiO_2[1$\bar{1}$0] azimuth due to the small width of the islands in that direction.

Additional structural characterization was performed using an Omicron LT-STM (low-temperature scanning tunneling microscope) equipped with an electron gun suitable for LEED and Auger electron spectroscopy (AES). The Ni crystal and the films were prepared following the same procedure as described above. This UHV system operated at a base pressure of 5×10^{-11} mbar.

3. Results and Discussion

3.1. The Phases Formed. *3.1.1. The Quasi-Hexagonal Phase.* A quasi-hexagonal phase described by the matrix $\begin{bmatrix} 1 & -3/7 \\ 0 & 6/7 \end{bmatrix}$ is obtained upon saturated oxidation of less than a monolayer equivalent (MLE, with 1 MLE corresponding to a coverage of 1 Ti atom per substrate surface unit cell) of Ti on Ni(110)[10] and was initially observed by Atrei et al. on $Ni_{94}Ti_6$(110).[2] The current model for this phase is a layer of titanium sandwiched between oxygen layers (Figure 1a). For the thin film formed on Ni(110) at MAX-lab, the LEED pattern (Figure 2a) is described by the matrix $\begin{bmatrix} 2 & -6/7 \\ 0 & 12/7 \end{bmatrix}$ (marked by "−" in Figure 2b), which is a (2 × 2) reconstruction of the Atrei et al. quasi-hexagonal phase.[2] Additionally, the extra spots on the half order of the Ni [1$\bar{1}$0] direction are most probably caused by a (2 × 1) oxygen reconstruction of the Ni substrate,[22] as the titanium coverage is too low to cover the entire surface. The LEED pattern obtained in this work is of higher quality than those in previous studies, indicating that the quasi-hexagonal structure proposed by Atrei et al. might not be the primary unit cell. Our unit cell is also twice that reported in our earlier STM investigation.[10] This discrepancy could arise from a *z*-direction relaxation of substrate atoms or thin film atoms not visible in the STM images.

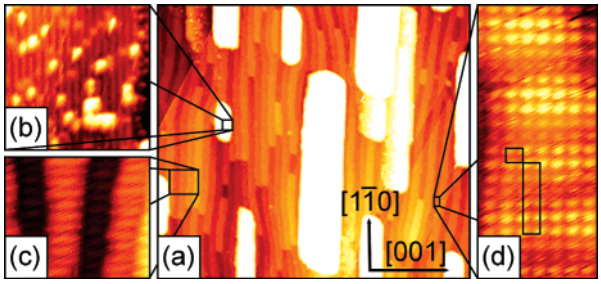

Figure 3. Topographic STM images of the rutile TiO_2 film. The film consists of 2.5 MLE of Ti annealed to 800 K for 30 min in 10^{-7} mbar of O_2. (a) Overview (2000 × 1750 Å^2; tunneling conditions: 1.30 V sample bias, 0.10 nA tunneling current). The symmetry of the Ni(110) substrate is indicated. (b) High-resolution image showing a TiO_2(110) island with the characteristic O vacancies and bridging OH groups (65 × 65 Å^2; tunneling conditions: 1.15 V sample bias, 0.1 nA tunneling current). (c) STM image of the wetting layer, showing the 40 Å periodicity along the [001] direction of the substrate (185 × 155 Å^2; tunneling conditions: 1.00 V sample bias, 1.00 nA tunneling current). (d) Atomically resolved image of the wetting layer. A (1 × 1) unit cell and a coincidence cell between the wetting layer and the substrate, resulting in a Moiré pattern, are indicated (35 × 60 Å^2; tunneling conditions: 0.64 V sample bias, 0.23 nA tunneling current). Images a−b recorded at 300 K; images c−d recorded at 78 K.

3.1.2. The Rutile TiO_2 Islands on the Wetting Layer of TiO_2. For higher Ti coverage (in the range of about 1−6 MLE[23]), under the same preparation conditions, it has been shown that three-dimensional rods of rutile TiO_2(110) grow on a wetting layer on top of Ni(110).[9] Figure 3 shows the STM topography of such a film. The film consists of 2.5 MLE of Ti annealed to 800 K for 30 min in 10^{-7} mbar of O_2. The coverage was estimated by calibration of the doser using Auger electron spectroscopy. The LEED pattern of this phase was described in ref 2 as showing a 5× periodicity with respect to the substrate in the [1$\bar{1}$0] direction, where not all five spots are evident on the LEED photograph, and with streaking along the [001] direction.

Careful inspection of the LEED patterns (Figure 2c,e) and the corresponding STM image (Figure 3d) allows us to determine the epitaxy matrix which describes the unit cell of this wetting phase layer with respect to the Ni substrate as $\begin{bmatrix} 6/5 & 0 \\ 0 & 1 \end{bmatrix}$. This results in a unit cell of 3.0 × 3.5 Å^2. In light of the STM evidence, these additional spots can be attributed either to the unit cell of the wetting layer and its multiple diffraction spots or to a coincidence cell between the wetting layer and the substrate. The LEED pattern of the same phase (Figure 2e−f), recorded on a different UHV system (LT-STM) at lower energy, reveals a splitting of the wetting layer unit cell spots. This splitting is consistent with a 40 ± 5 Å periodicity of the wetting layer in the substrate [001] direction, which is also visible in the corresponding STM image (Figure 3c). Hence, our wetting layer has a supercell of 15 × 40 Å^2. This phase had been assigned in previous work[9,10] to TiO(001) because of an inaccurate determination of the unit cell caused by STM drifting. The formation of nickel oxide phases was excluded based on the past HREELS measurements.[8] Given the additional accurate length determination that LEED can provide, we notice that the STM and LEED evidence for this phase is a close match to the wetting titania overlayer on (1 × 2)-Pt(110) recently reported by Orzali et al.[24] The latter, which has an overlayer unit cell of 3.0 × 3.9 Å^2, exhibits a 39 × 16 Å^2 supercell and can be described as a distorted anatase (001) bilayer. One should note that there is a 90° rotation of the overlayer supercell with respect to the substrate between our phase and the one reported for (1 × 2)-Pt(110). These differences probably arise due to the heteroepitaxial growth determined by the different substrate surfaces. On the basis of the above observations, Figure 1b illustrates a proposed atomic model for this wetting layer phase.

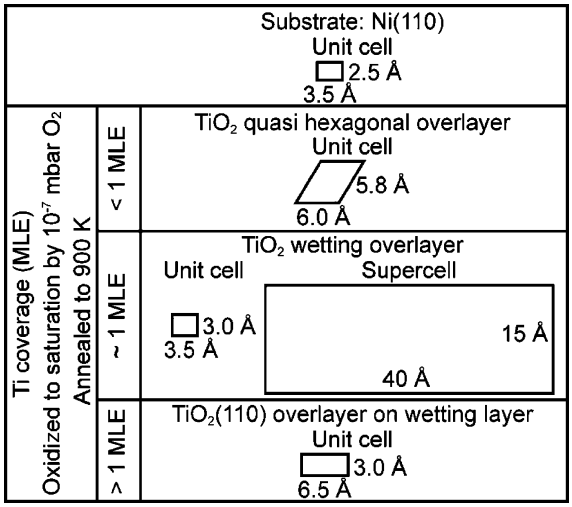

Figure 4. An illustration summarizing the TiO_2 phases investigated in this paper, indicating their unit cells and their preparation conditions.

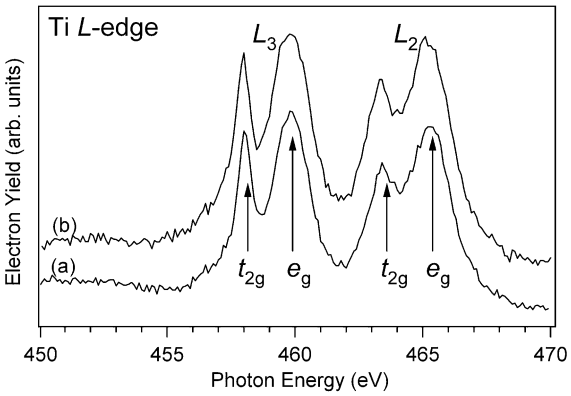

Figure 5. XANES over the Ti L-edge of (a) the thin film mainly of the quasi-hexagonal phase, consisting of subMLE Ti annealed to 800 K for 30 min in 10^{-7} mbar of O_2, and (b) the thin film with the rutile phase formed, consisting of 5 MLE of Ti oxidized for 1 min in 10^{-7} mbar of O_2 and annealed to 800 K. The spectra are offset for clarity.

The streaking of the LEED pattern along the substrate [001] direction is consistent with the width of the rutile rods being too small to reveal the periodicity along the TiO_2(110)−overlayer [1$\bar{1}$0] direction. The TiO_2(110) unit cell length along its [1$\bar{1}$0] direction is 6.5 Å compared with 3.5 Å for the wetting layer. Along the TiO_2(110) [001] direction, this phase is commensurate with the wetting layer. The LEED pattern of the film grown on beamline I311 is shown in Figure 2c, and it reveals additional diffuse spots of the quasi-hexagonal film (marked as "−" in Figure 2d), suggesting that this phase also forms on patches of the surface when the TiO_2(110) rods are present. This film was prepared by deposition of ~ 5MLE of Ti (as estimated by looking at the attenuation of the Ni $2p_{3/2}$ core levels after Ti deposition and assuming a close-packed structure of Ti) oxidized for 1 min in 10^{-7} mbar of O_2 and annealed to 800 K. Figure 4 summarizes the different phases discussed in this section, alongside with their corresponding unit cells and their preparation conditions.

3.2. XANES. XANES was employed to provide insight into the structure of the films. The results for the two films described above are shown in Figure 5. We notice that there are no obvious differences between the two spectra. X-ray absorption spectra over the Ti L-edge are reported for Ti metal,[25] TiO,[26] Ti_2O_3,[27]

$NiTiO_3$,[28] and anatase and rutile TiO_2[29] crystals and can be used as fingerprints in order to identify the phases of the film. Our spectra do not match any of the fingerprints closely enough for a definitive assignment.

The main conclusion that can be drawn from the XANES investigation is that the thin films are fully oxidized and that titanium is in the Ti^{4+} state. This is evident from the position of the L_3-edge, which is located at 458 eV.[30] This excludes the presence of Ti_2O_3 or other reduced phases. Also, we notice the characteristic splitting of the L_2- and the L_3-edge.

It has been shown by Okada and Kotani[31] that the L_2- and the L_3-edges in TiO_2 split into e_g and t_{2g} peaks separated by an energy of about 1.7 eV, assuming an octahedral symmetry. The first-neighbor O atoms are separated by the central Ti atom by 1.946 Å in the $(1\bar{1}0)$ plane and by 1.984 Å in the (110) plane; therefore, the resulting structure is a slightly distorted octahedron. The corresponding value for the TiO_2 films presented here is 1.8 ± 0.2 eV. Therefore, we deduce that titanium atoms are located in the center of distorted octahedra defined by O atoms at their corners.

In the XANES spectra of the Ti L-edge, there is a further splitting of the e_g component, which is usually resolved for the rutile and anatase phases of TiO_2. Kecheyev et al.[32] have recently reviewed the nature of this splitting. They argue that the most plausible mechanism proposed is associated with long-range order, although this is not fully elucidated. This would imply that interactions of Ti atoms with the second-neighbor shell are important, which will not be present for the quasi-hexagonal phase (Figure 5b). For the second film, where we have a mixture of rutile, wetting layer, and quasi-hexagonal phases, the absence of a splitting probably results from the surface heterogeneity.

3.3. SXPS. In an effort to establish the nature of the interaction between the substrate and the two ultrathin films, we looked at the evolution of the Ni $2p_{3/2}$ core level spectra. The spectrum of the clean metal is characterized by a main peak at 852.4 ± 0.1 eV and a satellite shifted 5.3 ± 0.1 eV toward higher binding energy from the main peak (Figure 6a). This satellite arises from final state effects that influence the core level spectra of Ni and its compounds.[33] These final states for the $2p_{3/2}$ core level are the core level hole, $2p^5_{3/2}3d^{10}$, and the hole generated within the valance band, localized on the photoion, $2p^5_{3/2}3d^9$.[34] The Ni $2p_{3/2}$ spectrum of NiO is somewhat more complicated, with the appearance of nonlocal screening effects, which are described in detail in ref 35.

Spectra b and c in Figure 6 show the Ni $2p_{3/2}$ spectra of the substrate after growing the rutile and the quasi-hexagonal film, respectively. Careful examination of the spectra recorded from our films shows subtle changes with respect to the clean surface signal, which indicate that the nickel substrate does not remain inert upon the formation of the thin films. For comparison, the effect of the chemisorption of O_2 on Ni(110) on the peak shape of the Ni $2p_{3/2}$ core level as a function of O_2 coverage is shown in Figure 6d−f.[36] The effect of the oxygen chemisorption is manifested by the reduction of the satellite intensity and the additional appearance of new core level states between the main Ni $2p_{3/2}$ peak and its satellite. These changes differ from those observed on the formation of bulk-like NiO.[36] The changes observed upon oxygen chemisorption of up to ~1 ML on Ni(110) are comparable to the changes observed in our Ni spectra after the deposition of the ultrathin films, suggesting that they are caused by oxygen at the interface. Since these changes are observed for both films, it seems unlikely that they arise solely from O_2-induced reconstruction of Ni(110), which is evidenced only in the LEED pattern of the surface containing the quasi-hexagonal film. The film containing TiO_2(110) rods does not expose the Ni(110) substrate.

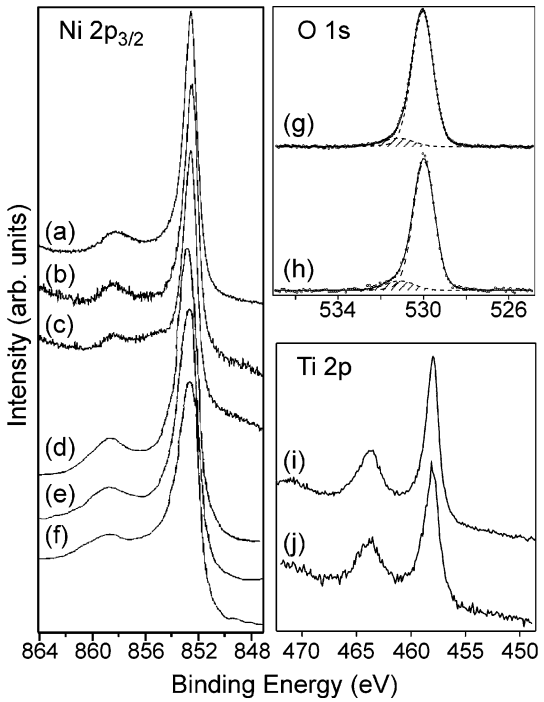

Figure 6. Left panel: Ni $2p_{3/2}$ XPS spectra ($h\nu = 1000$ eV) of Ni(110) (a) clean surface, (b) with the rutile film, and (c) with the quasi-hexagonal film. Ni $2p_{3/2}$ XPS spectra adapted from Norton et al.[36] of Ni(110) (d) clean surface, (e) with a ~0.44 ML coverage of chemisorbed oxygen at 295 K, and (f) with a ~1.00 ML coverage of chemisorbed oxygen at 295 K. The spectra are peak-height normalized and offset for clarity. Top right panel: O 1s XPS spectra ($h\nu = 650$ eV) (g) of the quasi-hexagonal film and (h) of the rutile film. Circles, dashed lines, and solid lines denote the data points, the different components of the fit, and the sum of the components, respectively. The feature appearing at a shift of 1.13 eV from the bulk oxygen contribution is attributed to OH species. The full-width at half-maximum (FWHM) of the Gaussian contribution to the components is 1.1 and 1.45 eV for the main peak and the OH contribution, respectively. All components have a Lorentzian contribution with a FWHM of 0.14 eV. The background has been subtracted from the spectra. The spectra are offset for clarity. Bottom right panel: Ti 2p XPS spectra ($h\nu = 680$ eV) (i) of the quasi-hexagonal film and (j) of the rutile film. The spectra are offset and normalized to the Ti $2p_{3/2}$ for clarity.

The attenuation of the intensity of the Ni $2p_{3/2}$ core level under the films was used in order to provide an estimate of the film thickness. This method has an estimated accuracy of ±50%. At normal emission, these are related by

$$d = -\lambda(E) \ln \frac{I_i}{I_0}$$

where d is the thickness of the film, $\lambda(E)$ is the electron attenuation length of electrons at kinetic energy E, I_i is the intensity of the substrate after the deposition of film i, and I_0 is the intensity of the clean substrate. For $h\nu = 1000$ eV, Ni $2p_{3/2}$ photoelectrons have kinetic energies of approximately 150 eV and electron attenuation lengths of about 7−8 Å.[37] Hence, we find that the rutile film has an effective thickness of 6.5−10.0 Å.

The oxygen O 1s peak for the ultrathin films is located at 530.00 ± 0.15 eV. This coincides with the reported value for bulk titanium dioxide.[38] A satellite at a higher binding energy of 1.18−1.33 eV appears for the (110) rutile surface.[16,17] It has been shown that this satellite increases at grazing emission

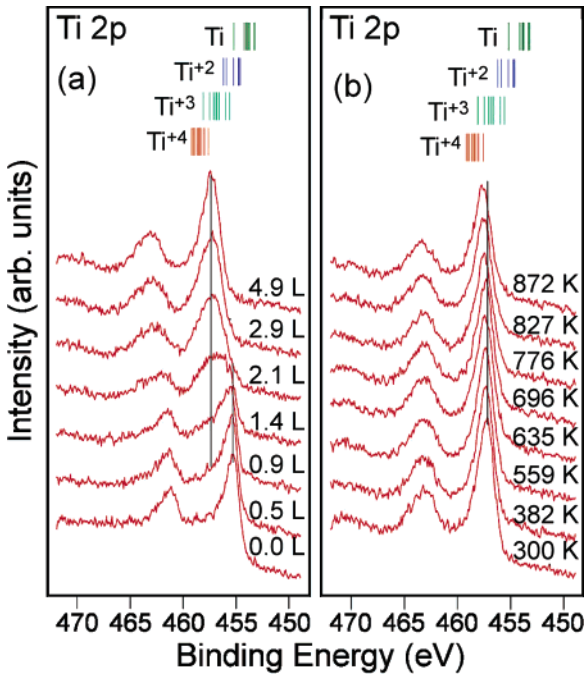

Figure 7. Ti 2p XPS spectra ($h\nu = 680$ eV). (a) The oxidation of the thin film; the oxygen exposure is noted over each spectrum. (b) The annealing of the thin film; the annealing temperature is noted over each spectrum. The spectra are offset for clarity. At the top, the bars display literature positions for Ti $2p_{3/2}$ core level binding energies for different oxidation states of titanium.[5,38]

angles, and it has been attributed to the surface, twofold, bridging oxygen atoms.[16,17] The satellite appears for both of our films, with slightly different intensity (see Figure 6g−h), 9% of the main peak for the quasi-hexagonal film and 10% of the main peak for the film with rutile phase. As we do not expect bridging oxygen atoms in the case of the quasi-hexagonal phase, we suggest instead that it may originate from OH species, resulting from the interaction of the film with the residual H_2O in the UHV system. This assignment is discussed below in relation to the reactivity of the ultrathin rutile film.

Titanium 2p core levels of the ultrathin films are shown in Figure 6i−j. The final oxidation state of titanium is very similar for both phases. Our films reach the highest oxidation state when the Ti $2p_{3/2}$ core level peak has shifted to 458 eV. This value is at the lower limit of the reported values for Ti^{4+}.[5,38] The spin−orbit splitting of the Ti 2p core levels is 5.81 eV, which is within the published values for TiO_2.[38] The shape of the Ti 2p peak of the rutile thin film also matches that reported from the bulk crystal.[39] The full-width at half-maximum of this peak is measured to be 1.60 ± 0.04 eV for the quasi-hexagonal phase and 1.70 ± 0.04 eV for the film with rutile present. It should be noted that there is still some quasi-hexagonal phase on the latter surface, which might explain this broadening. The reported satellites of the Ti 2p peak for rutile TiO_2(110) at about 3 and 13 eV[40] are present on both films.

The Ti 2p XPS spectrum of the thin film does not have a contribution due to TiO. This is evident by looking in the band of the reported binding energies for Ti^{2+} (454.6−456.1 eV) (Figure 7b). Additionally, the electronic structure of fcc TiO was shown by Bartkowski et al.[42] to be consistent with the Doniach− Ŝunjić shape, as would be expected from its metallic character. This is not evident in the Ti 2p spectrum of the rutile ultrathin film. These observations further support the reassignment of the pseudosquare cell[9,23,41] wetting layer to anatase-like TiO_2(001).

The oxidation of the rutile film was further investigated using SXPS measurements of the Ti 2p core level during exposure of the Ti overlayer to oxygen. The preparation procedure was separated into oxidation and annealing stages, that is, instead of annealing in an O_2 environment, the deposited titanium was initially oxidized and subsequently annealed. The two different procedures produced the same LEED pattern. We notice that after the deposition of titanium, carbon and oxygen contamination is present, evidenced by the appearance of C 1s and O 1s core level peaks. It should also be noted that there is no carbon contamination detected by XPS after Ti oxidation. The position of the as-deposited Ti $2p_{3/2}$ peak is at 455.1 ± 0.1 eV, which suggests that titanium is already partly oxidized and, more particularly, in the Ti^{2+} state,[43] judging from the peak shift from the fully oxidized position. The corresponding spectrum (bottom spectrum in Figure 7a) shows that the film has metallic character, obvious by an asymmetry which is not present on the fully oxidized film.

The surface is saturated by oxygen after an exposure to O_2 of less than 5 L (Figure 7a), with the final Ti $2p_{3/2}$ located at a binding energy higher by 2.4 ± 0.1 eV. After exposure of about 1 L of O_2, we notice the appearance of a new peak at 457.5 ± 0.1 eV. This grows with increasing exposure, while the peak of the as-deposited titanium gradually decreases and finally disappears after about 3 L of O_2.

Subsequently, the film was annealed in situ to 900 K, a gradual shift of the Ti $2p_{3/2}$ peak up to 0.5 eV higher binding energy being observed, until it reached the value of 458.0 ± 0.1 eV, a close match to the reported value for bulk TiO_2 (458.5 eV).[5,38] No new peaks appeared during the annealing process (see Figure 7b). This is consistent with the XPS measurements of Biener et al.[44] on the formation of ordered TiO_2 structures on Au(111). In their case, after deposition of a titanium layer, which was subsequently oxidized, the Ti 2p core level shifted 1.3 eV toward higher binding energy upon annealing. This phenomenon seems to be characteristic of the oxidation of titanium under these conditions.

3.4. Reactivity of the TiO_2(110) Ultrathin Film. Water was dosed at about 190 K on the thin film with the rutile phase present. According to Henderson,[13] a water multilayer does not form on TiO_2(110) at temperatures above 180 K. The initial exposure was carried out at a pressure of 4×10^{-8} mbar. After an exposure to about 160 L of H_2O, two new features appeared in the O 1s spectrum, at 1.13 ± 0.10 and 3.00 ± 0.10 eV toward higher binding energy (Figure 8a). There is ambiguity in the literature concerning the identification of the O 1s core level spectrum of OH and molecular H_2O resulting from exposure of TiO_2(110) to H_2O.[12,14,16,17,45,46] The current consensus on the peak assignment is that the O 1s peak due to hydroxyls appears at lower binding energy than that for water. Considering other oxides, such as α-Al_2O_3(0001), α-Fe_2O_3(0001), Fe_3O_4(111), and MgO(100), the feature appearing at 1.2−2.5 eV higher with respect to bulk O 1s is assigned to OH. The feature at 2.5−3.5 eV higher binding energy is assigned to H_2O.[47,48] Wang et al.,[46] who recorded the O 1s core level of TiO_2 after both liquid and vapor exposure to water at room temperature, assigned a feature at 1.6 eV higher binding energy to OH species. More recently, Allegretti et al.[14] used photoelectron diffraction combined with SXPS to show that molecularly adsorbed water on TiO_2(110) appears at 3.2−3.6 eV higher binding energy with respect to the bulk O 1s peak. Also according to Allegretti et al., only molecularly adsorbed water should be stable on single-crystal TiO_2(110) at 190 K.[14] Taking the above into consideration, it is reasonable to assign the two adsorbate-induced O 1s peaks

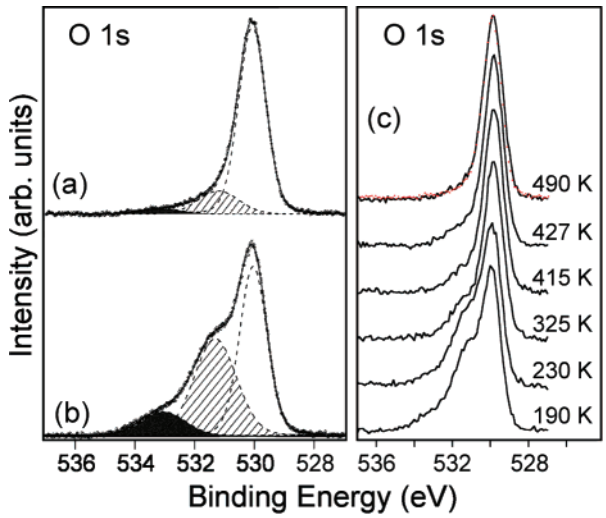

Figure 8. O 1s core level spectra ($h\nu = 650$ eV) of the rutile ultrathin film (a) after 160 L exposure of H_2O recorded at 190 K and (b) after high-pressure (2×10^{-6} mbar) H_2O exposure recorded at 190 K. Circles, dashed lines, and the solid line denote the data points, the different components of the fit, and the sum of the components, respectively. The background has been subtracted from the spectrum. The contribution of the molecular water on the spectrum is highlighted in gray at a shift of 3 eV from the O 1s bulk contribution. The contribution of hydroxyls is highlighted by diagonal lines at a shift of (a) 1.13 eV and (b) 1.27 eV from the O 1s bulk contribution. The FWHM of the Gaussian contribution to the components is 1 eV for the bulk, (a) 1.54 eV and (b) 1.59 eV for the OH and (a) 1.55 eV and (b) 1.63 eV for the H_2O contributions. All components have a Lorentzian contribution with a FWHM of 0.14 eV. (c) Solid lines correspond to annealing after the high-pressure H_2O exposure. The respective annealing temperatures are noted on their right. The dashed line corresponds to the rutile film before exposure to H_2O; it is displayed for comparison alongside the spectrum of the film annealed to 490 K.

in our spectra to the coexistence of surface hydroxyl and water molecules with an intensity ratio of about 4:1, respectively. It is possible that the hydroxyl component arises from reaction of H_2O with the exposed wetting layer. It is worth noting that ab initio calculations predict the dissociation of H_2O on anatase TiO_2(001) for a H_2O coverage less than 0.5 per Ti site and the coexistence of molecular and dissociated H_2O with a 1:1 ratio for higher H_2O coverage.[49]

By increasing the H_2O pressure to 2×10^{-6} mbar, we observed the hydroxylation of the thin film. A similar effect was observed for the single-crystal TiO_2 surface by Bullock et al.[17] Figure 8b depicts the O 1s spectrum after this high water pressure exposure. We noticed a dramatic increase in the hydroxyl peak, along with the corresponding increase in the molecular water contribution. By looking into the attenuation of the O 1s peak due to the TiO_2 film, we estimated that the mixed water/hydroxyl overlayer has an average thickness of 0.6−3.5 Å. The intensity ratio of the OH to H_2O components remained 4:1. Assuming that the OH has a bond length of about 1 Å and that H_2O has a height of about 1.5 Å, this gives an estimation of the coverage of the mixed overlayer being 0.5−3.2 ML. The greater width of the Gaussian contribution of the OH and H_2O peaks can be attributed to the formation of a H-bonded structure. Alternatively, it could be due to occupation of additional adsorption sites, such as the step edges and the sides of the three-dimensional rutile rods. The presence of the O 1s contribution due to the TiO_2 film indicates that hydroxylation is not complete throughout the ultrathin film.

Finally, we annealed the hydroxylated film while monitoring the O 1s spectrum. We observed that the adsorbate-induced features gradually decrease until they are completely removed by annealing at 490 ± 15 K (Figure 8c). Hence, we deduce that the hydroxylation process is reversible. The film was further annealed to 525 K and subsequently cooled down to 190 K to confirm that there were no additional changes to the O 1s spectrum.

4. Conclusions

The growth of fully oxidized titanium films on the Ni(110) surface has been examined using core level SXPS and XANES. LEED was used to identify the films and link them to previous studies of this system. We confirm that these consist of a rutile TiO_2(110) film, as described by Ashworth et al.,[9] and a quasi-hexagonal overlayer phase described in matrix notation by $\begin{bmatrix} 2 & -6/7 \\ 0 & 12/7 \end{bmatrix}$. We suggest that oxygen lies at the interface between the oxide and the metal based on the Ni $2p_{3/2}$ core level spectra. We have also used XPS and XANES to follow the oxidation procedure and deduce that our films consist of fully oxidized titanium. By dosing water on to the rutile and wetting layer film at 10^{-8} mbar, we observe the coadsorption of both molecular water and hydroxyl groups, with the appearance of two new features in the O 1s core level spectrum. Hydroxylation of the thin film is observed following exposure to 10^{-6} mbar of H_2O. Finally, we show that the process of hydroxylation is reversible after annealing to 490 K.

Acknowledgment. We would like to thank Dr. Chi Lun Pang for useful discussions, Dr. Gilberto Teobaldi for the computer model of the TiO_2 wetting layer on Ni(110), and the MAX-lab staff for their support. This work was funded by the EPSRC (U.K.), the Swedish Research Council, and the EU through the STRP project NanoChemSens (Contract STRP 505895-1). The use of the synchrotron radiation facilities was provided by the EU Transnational Access to Research Infrastructures within the Integrating Activity on Synchrotron and Free Electron Laser Science (IA-SFS).

References and Notes

(1) Freund, H.-J.; Kuhlenbeck, H.; Staemmler, V. *Rep. Prog. Phys.* **1996**, *59*, 283.
(2) Atrei, A.; Bardi, U.; Rovida, G. *Surf. Sci.* **1997**, *391*, 216.
(3) Dulub, O.; Hebenstreit, W.; Diebold, U. *Phys. Rev. Lett.* **2000**, *84*, 3646.
(4) Bennett, R. A.; Pang, C. L.; Perkins, N.; Smith, R. D.; Morrall, P.; Kvon, R. I.; Bowker, M. *J. Phys. Chem. B* **2002**, *106*, 4688.
(5) Sedona, F.; Rizzi, G. A.; Agnoli, S.; Llabrés i Xamena, F. X.; Papageorgiou, A.; Ostermann, D.; Sambi, M.; Finetti, P.; Schierbaum, K.; Granozzi, G. *J. Phys. Chem. B* **2005**, *109*, 24411.
(6) Schoiswohl, J.; Tzvetkov, G.; Pfuner, F.; Ramsey, M. G.; Surnev, S.; Netzer, F. P. *Phys. Chem. Chem. Phys.* **2006**, *8*, 1614.
(7) Diebold, U. *Surf. Sci. Rep.* **2003**, *48*, 53.
(8) Chang, Z.; Thornton, G. *Surf. Sci.* **2000**, *462*, 68.
(9) Ashworth, T. V.; Thornton, G. *Thin Solid Films* **2001**, *400*, 43.
(10) Ashworth, T. V.; Muryn, C. A.; Thornton, G. *Nanotechnology* **2005**, *16*, 3041.
(11) Lindan, P. J. D.; Zhang, C. *Phys. Rev. B* **2005**, *72*, 75439.
(12) Henderson, M. A. *Surf. Sci. Rep.* **2002**, *46*, 1.
(13) Henderson, M. A. *Surf. Sci.* **1996**, *355*, 151.
(14) Allegretti, F.; O'Brien, S.; Polcik, M.; Sayago, D. I.; Woodruff, D. P. *Phys. Rev. Lett.* **2005**, *95*, 226104.
(15) Bikondoa, O.; Pang, C. L.; Ithnin, R.; Muryn, C. A.; Onishi, H.; Thornton, G. *Nat. Mater.* **2006**, *5*, 189.
(16) Sham, T. K.; Lazarus, M. S. *Chem. Phys. Lett.* **1979**, *68*, 426.
(17) Bullock, E. L.; Patthey, L.; Steinemann, S. G. *Surf. Sci.* **1996**, *352*, 504.
(18) Nyholm, R.; Andersen, J. N.; Johansson, U.; Jensen, B. N.; Lindau, I. *Nucl. Instrum. Methods Phys. Res., Sect. A* **2001**, *467*, 520.
(19) Doniach, S.; Šunjić, M. *J. Phys. C: Solid State Phys.* **1970**, *3*, 285.
(20) Shirley, D. A. *Phys. Rev. B* **1972**, *5*, 4709.
(21) Weissenrieder, J.; Mikkelsen, A.; Andersen, J. N.; Feibelman, P. J.; Held, G. *Phys. Rev. Lett.* **2004**, *93*, 196102.

(22) Eierdal, L.; Besenbacher, F.; Lægsgaard, E.; Stensgaard, I. *Surf. Sci.* **1994**, *312*, 31.
(23) Ashworth, T. V. Ph.D. Thesis, University of Manchester, 2003.
(24) Orzali, T.; Casarin, M.; Granozzi, G.; Sambi, M.; Vittadini, A. *Phys. Rev. Lett.* **2006**, *97*, 156101.
(25) Fink, J.; Müller-Heinzerling, Th.; Scheerer, B.; Speier, W.; Hillebrecht, F. U.; Fuggle, J. C.; Zaanen, J.; Sawatzky, G. A. *Phys. Rev. B* **1985**, *32*, 4899.
(26) Lusvardi, V. S.; Barteau, M. A.; Chen, J. G.; Eng, J., Jr.; Frühberger, B.; Teplyakov, A. *Surf. Sci.* **1998**, *397*, 237.
(27) Uozumi, T.; Okada, K.; Kotani, A.; Tezuka, Y.; Shin, S. *J. Phys. Soc. Jpn.* **1996**, *65*, 1150.
(28) Soriano, L.; Abbate, M.; Fernández, A.; González-Elipe, A. R.; Sanz, J. M. *Surf. Interface Anal.* **1997**, *25*, 804.
(29) van der Laan, G. *Phys. Rev. B* **1990**, *41*, 12366.
(30) Yoshiya, M.; Tanaka, I.; Kaneko, K.; Adachi, H. *J. Phys.: Condens. Matter* **1999**, *11*, 3217.
(31) Okada, K.; Kotani, A. *J. Electron Spectrosc. Relat. Phenom.* **1993**, *62*, 131.
(32) Kucheyev, S. O.; van Buuren, T.; Baumann, T. F.; Satcher, J. H., Jr.; Willey, T. M.; Meulenberg, R. W.; Felter, T. E.; Poco, J. F.; Gammon, S. A.; Terminello, L. J. *Phys. Rev. B* **2004**, *69*, 245102.
(33) Hüfner, S. *Photoelectron Spectroscopy*; 3rd ed.; Springer: Berlin, Germany, 2003.
(34) van der Laan, G.; Thole, B. T. *J. Phys.: Condens. Matter* **1992**, *4*, 4181.
(35) van Veenendaal, M. A.; Sawatzky, G. A. *Phys. Rev. Lett.* **1993**, *70*, 2459.
(36) Norton, P. R.; Tapping, R. L.; Goodale, J. W. *Surf. Sci.* **1977**, *65*, 13.
(37) Woodruff, D. P.; Delchar, T. A. *Modern Techniques of Surface Science*; 2nd ed.; Cambridge University Press: Cambridge, U.K., 1994.
(38) NIST X-ray Photoelectron Spectroscopy Database; NIST Standard Reference Database 20, Version 3.4 (Web Version). http://srdata.nist.gov/xps/.
(39) Sen, S. K.; Riga, J.; Verbist, J. *Chem. Phys. Lett.* **1976**, *39*, 560.
(40) Oku, M.; Matsuta, H.; Wagatsuma, K.; Waseda, Y.; Kohiki, S. *J. Electron Spectrosc. Relat. Phenom.* **1999**, *105*, 211.
(41) Leung, L. Ph.D. Thesis, University of Manchester, 2005.
(42) Bartkowski, S.; Neumann, M.; Kurmaev, E. Z.; Fedorenko, V. V.; Shamin, S. N.; Cherkashenko, V. M.; Nemnonov, S. N.; Winiarski, A.; Rubie, D. C. *Phys. Rev. B* **1997**, *56*, 10656.
(43) Mayer, J. T.; Diebold, U.; Madey, T. E.; Garfunkel, E. *J. Electron Spectrosc. Relat. Phenom.* **1995**, *73*, 1.
(44) Biener, J.; Farfan-Arribas, E.; Biener, M.; Friend, C. M.; Madix, R. J. *J. Chem. Phys.* **2005**, *123*, 094705.
(45) Cardenas, J.; Sjöberg, S. *Surf. Sci.* **2003**, *532*, 1104.
(46) Wang, L.-Q.; Baer, D. R.; Engelhard, M. H.; Shultz, A. N. *Surf. Sci.* **1995**, *344*, 237.
(47) Kendelewicz, T.; Liu, P.; Doyle, C. S.; Brown, G. E., Jr.; Nelson, E. J.; Chambers, S. A. *Surf. Sci.* **2000**, *453*, 32.
(48) Liu, P.; Kendelewicz, T.; Brown, G. E., Jr.; Nelson, E. J.; Chambers, S. A. *Surf. Sci.* **1998**, *417*, 53.
(49) Vittadini, A.; Selloni, A.; Rotzinger, F. P.; Grätzel, M. *Phys. Rev. Lett.* **1998**, *81*, 2954.